Nonlinear Dyn (2012) 69:57–70
DOI 10.1007/s11071-011-0245-6

ORIGINAL PAPER

Bifurcation analysis of an aeroelastic system with concentrated nonlinearities

Abdessattar Abdelkefi · Rui Vasconcellos · Flavio D. Marques · Muhammad R. Hajj

Received: 8 May 2011 / Accepted: 6 October 2011 / Published online: 10 November 2011

Abstract Analytical and numerical analyses of the nonlinear response of a three-degree-of-freedom nonlinear aeroelastic system are performed. Particularly, the effects of concentrated structural nonlinearities on the different motions are determined. The concentrated nonlinearities are introduced in the pitch, plunge, and flap springs by adding cubic stiffness in each of them. Quasi-steady approximation and the Duhamel formulation are used to model the aerodynamic loads. Using the quasi-steady approach, we derive the normal form of the Hopf bifurcation associated with the system's instability. Using the nonlinear form, three configurations including supercritical and subcritical aeroelastic systems are defined and analyzed numerically. The characteristics of these different configurations in terms of stability and motions are evaluated. The usefulness of the two aerodynamic formulations in the prediction of the different motions beyond the bifurcation is discussed.

Keywords Nonlinear aeroelasticity · Quasi-steady · Duhamel formulation · Normal form

A. Abdelkefi · M.R. Hajj (✉)
Virginia Tech, Blacksburg, VA, USA
e-mail: mhajj@vt.edu

R. Vasconcellos · F.D. Marques
University of Sao Paulo, Sao Carlos, Brazil

1 Introduction

Complex aeroelastic phenomena, such as flutter, limit-cycle oscillations (LCOs), chaos and bifurcations, affect the performance of the aircraft and may result in structural problems and material fatigue [1–3]. Such phenomena are associated with nonlinear aerodynamic or structural conditions that characterize aeroelastic systems. Regarding structural nonlinearities, they can arise from large structural deflections and/or partial loss of structural integrity [4–7]. Furthermore, the effects of aging, loose attachments, and material features could lead to undesirable and dangerous responses [8–10]. As such, assessing the evolution of these inevitable behaviors through modeling and analysis of these nonlinearities is important to avoid or control dangerous responses. LCOs associated with nonlinearities in aeroelastic systems have been proposed for energy harvesting [11]. In these applications, it is important to exploit nonlinearities to maximize harvested power. These nonlinearities can be classified into either distributed or concentrated, based on the region of their existence. Distributed nonlinearities arise generally from deformations of the entire structure. On the other hand, concentrated nonlinearities arise from loose or worn hinges of control surfaces. In this work, we focus on the concentrated nonlinearities which can be modeled using nonlinear springs in the plunge, pitch, and control surface motions.

Analytically, the aerodynamic loads are usually modeled using the quasi-steady approximation [1] or

the Duhamel formulation [12, 13]. These approximations are based on the Theodorsen approach for the unsteady aerodynamic loads. In the quasi-steady approximation, the lag between the unsteady oscillations and their effects on aerodynamic force and torques is neglected and therefore it is only limited to relatively low-frequency oscillations, i.e. small values of reduced frequencies. On the other hand, the Duhamel formulation could simulate arbitrary motions of the airfoil. Generally, the Duhamel approximation has been used to study the effects of freeplay nonlinearity on the motions of control surfaces [2, 9, 10, 12] which has been shown to result in chaotic motions at speeds lower than the linear flutter speed.

The ability to determine contributions by different structural nonlinearities to the system's response allows for control and possibly elimination of subcritical instabilities. Furthermore, it is important to determine global response parameters. Such parameters and their relation (e.g. frequency ratios of different motions) would depend on accurate representation of the underlying physics such as aerodynamic loads, stiffness, damping, etc. In this work, we perform analysis of different nonlinear aeroelastic systems using two approximations of the aerodynamic loads. The objectives are to show how global analysis yields relevant characterization of the system and to present the shortcomings of using the quasi-steady approximation for specific aeroelastic systems. As such, the aeroelastic response of a three-degree-of-freedom airfoil section with concentrated structural nonlinearities is considered. In Sect. 2, the equations of motion of this aeroelastic system are presented. In Sect. 3, different representations of the aerodynamic loads, namely, the quasi-steady approximation and the Duhamel formulation, are implemented. In Sect. 4, the normal form of Hopf bifurcation is derived to obtain analytical expressions for the steady-state plunge, pitch, and flap motions. In Sect. 5, a comparison between the used aerodynamic loads approaches is determined for different considered configurations. Conclusions are presented in Sect. 6.

2 Representation of the aeroelastic system

We consider a two-dimensional rigid airfoil constrained to three degrees of freedom; namely, the plunge (w), pitch (α) and control surface flap (β) motions as shown in Fig. 1. The equations of motion of the system are written as [1]:

$$\begin{bmatrix} m_T & m_W b x_\alpha & m_W b x_\beta \\ m_W b x_\alpha & m_W b^2 r_\alpha^2 & m_W b^2 r_\beta^2 + m_W b^2 x_\beta (c-a) \\ m_W b x_\beta & m_W b^2 r_\beta^2 + m_W b^2 x_\beta (c-a) & m_W b^2 r_\beta^2 \end{bmatrix} \begin{bmatrix} \ddot{w} \\ \ddot{\alpha} \\ \ddot{\beta} \end{bmatrix} + \begin{bmatrix} d_w & 0 & 0 \\ 0 & d_\alpha & 0 \\ 0 & 0 & d_\beta \end{bmatrix} \begin{bmatrix} \dot{w} \\ \dot{\alpha} \\ \dot{\beta} \end{bmatrix} + \begin{bmatrix} k_w(w) & 0 & 0 \\ 0 & k_\alpha(\alpha) & 0 \\ 0 & 0 & k_\beta(\beta) \end{bmatrix} \begin{bmatrix} w \\ \alpha \\ \beta \end{bmatrix} = \begin{bmatrix} L \\ M_\alpha \\ M_\beta \end{bmatrix} \tag{1}$$

where

$$x_\alpha = \frac{S_\alpha}{m_W b}; \qquad x_\beta = \frac{S_\beta}{m_W b};$$
$$r_\alpha^2 = \frac{I_\alpha}{m_W b^2}; \qquad r_\beta^2 = \frac{I_\beta}{m_W b^2};$$

and m_W is the mass of the wing, m_T is the mass of the entire system (wing + support blocks); d_w, d_α and d_β are damping coefficients for the plunge, pitch, and flap motions, respectively. Furthermore, I_α is the airfoil mass moment of inertia about the elastic axis and I_β is the control surface mass moment of inertia about the elastic axis.

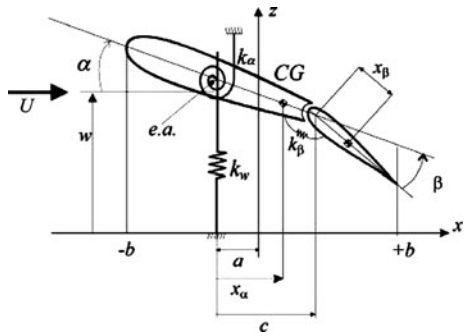

Fig. 1 Structural representation of the aeroelastic model

The plunge and pitch motions are measured at the elastic axis and the β angle of the control surface is measured at the hinge line. In addition, c represents the distance between the elastic axis to the hinge line of control surface, b is the semichord of the entire airfoil section. The mass center of the entire airfoil is located at a distance x_α from the elastic axis and the mass center of the control surface is located at a distance x_β from the hinge line. Further, k_w represents the plunge stiffness, k_α the stiffness of the pitch spring, k_β the stiffness of the control surface hinge. Furthermore, L and M_α are the aerodynamic lift and moment measured about the elastic axis and M_β is the aerodynamic moment on the flap about the flap hinge; S_α and S_β are the static mass moments.

For this work, we consider only structural nonlinearities. In addition, we consider a specific type of concentrated nonlinearity whereby hard and soft nonlinear springs are used to represent the stiffness of the different motions. These nonlinearities are modeled by cubic terms, i.e.

$$\begin{aligned} k_w &= k_{w0} + k_{w2} w^2 \\ k_\alpha &= k_{\alpha 0} + k_{\alpha 2} \alpha^2 \\ k_\beta &= k_{\beta 0} + k_{\beta 2} \beta^2 \end{aligned} \tag{2}$$

3 Representation of aerodynamic loads

In this work, we use the aerodynamic lift and moments as derived by Theodorsen [13], which are written as

$$\begin{aligned} L = &-\pi\rho b^2 \left[\ddot{w} + U\dot{\alpha} - ba\ddot{\alpha} - \frac{U}{\pi} T_4 \dot{\beta} - \frac{b}{\pi} T_1 \ddot{\beta} \right] \\ &- 2\pi\rho U b Q C(k) \end{aligned} \tag{3}$$

$$\begin{aligned} M_\alpha = &\pi\rho b^2 \left[ba\ddot{w} - Ub\left(\frac{1}{2} - a\right)\dot{\alpha} - b^2\left(\frac{1}{8} + a^2\right)\ddot{\alpha} \right. \\ &- \frac{U^2}{\pi}(T_4 + T_{10})\beta \\ &+ \frac{Ub}{\pi}\left\{ -T_1 + T_8 + (c-a)T_4 - \frac{1}{2}T_{11} \right\}\dot{\beta} \\ &\left. + \frac{b^2}{\pi}\left\{ T_7 + (c-a)T_1 \right\}\ddot{\beta} \right] \\ &+ 2\pi\rho b^2 U \left(a + \frac{1}{2}\right) Q C(k) \end{aligned} \tag{4}$$

and

$$\begin{aligned} M_\beta = &\pi\rho b^2 \left[\frac{b}{\pi} T_1 \ddot{w} + \frac{Ub}{\pi} \left\{ 2T_9 + T_1 \right. \right. \\ &\left. - \left(a - \frac{1}{2}\right) T_4 \right\} \dot{\alpha} - \frac{2b^2}{\pi} T_{13} \ddot{\alpha} \\ &- \left(\frac{U}{\pi}\right)^2 (T_5 - T_4 T_{10})\beta \\ &\left. + \frac{Ub}{2\pi^2} T_4 T_{11} \dot{\beta} + \left(\frac{b}{\pi}\right)^2 T_3 \ddot{\beta} \right] \\ &- \rho U b^2 T_{12} Q C(k) \end{aligned} \tag{5}$$

where

$$Q = U\alpha + \dot{w} + \dot{\alpha} b\left(\frac{1}{2} - a\right) + \frac{U}{\pi} T_{10}\beta + \frac{b}{2\pi} T_{11}\dot{\beta} \tag{6}$$

and T functions are defined in Appendix A.

Clearly, the aerodynamic loads are dependent on Theodorsen's function $C(k)$, where $k = \frac{wb}{U}$ is the reduced frequency of the harmonic oscillations. The exact expression of $C(k)$ is given by [1]:

$$C(k) = F(k) + iG(k) \tag{7}$$

where F and G are the function of Hankel and the modified Bessel function.

3.1 Quasi-steady approximation

In the quasi-steady approximation, the reduced frequency approaches zero and $C(k)$ is set equal to one. This assumption neglects any lag between the unsteady oscillations and their effects on aerodynamic forces and torques, limiting the modeling capabilities to relatively low-frequency oscillations. Setting $C(k) = 1$, we obtain second-order equations of motion with only structural cubic nonlinearity. The general form of these equations of motion is then written as

$$M\ddot{q} + C\dot{q} + Kq + N(q, q, q) = 0 \tag{8}$$

where

$$q = \begin{bmatrix} w \\ \alpha \\ \beta \end{bmatrix}, \tag{9}$$

$$M = \begin{bmatrix} m_T + \pi\rho b^2 & S_\alpha - a\pi\rho b^3 & S_\beta - T_1\rho b^3 \\ S_\alpha - a\pi\rho b^3 & I_\alpha + \pi(\frac{1}{8} + a^2)\rho b^2 & I_\beta + b(c-a)S_\beta + 2T_{13}\rho b^4 \\ S_\beta - T_1\rho b^3 & I_\beta + b(c-a)S_\beta + 2T_{13}\rho b^4 & I_\beta - \frac{T_3}{\pi}\rho b^4 \end{bmatrix}, \tag{10}$$

$$C = \begin{bmatrix} d_w + 2\pi\rho bU & 2(1-a)\pi\rho b^2 U & (T_{11} - T_4)\rho U b^2 \\ -2\pi(a + \frac{1}{2})\rho b^2 U & d_\alpha + a(2a-1)\pi\rho b^3 U & [T_1 - T_8 - (c-a)T_4 - aT_{11}]\rho b^3 U \\ T_{12}\rho b^2 U & [T_4(a - \frac{1}{2}) - T_1 - 2T_9 + T_{12}(\frac{1}{2} - a)]\rho b^3 U & d_\beta + [T_{11}T_{12} - T_4 T_{11}]\frac{\rho}{2\pi} b^3 U \end{bmatrix}, \tag{11}$$

$$K = \begin{bmatrix} k_{w0} & 2\pi\rho bU^2 & 2\rho bU^2 T_{10} \\ 0 & k_{\alpha 0} - 2\pi(\frac{1}{2} + a)\rho b^2 U^2 & [T_4 - 2aT_{10}]\rho b^2 U^2 \\ 0 & T_{12}\rho b^2 U^2 & k_{\beta 0} + (T_5 - T_4 T_{10} + T_{10}T_{12})\frac{\rho}{\pi} b^2 U^2 \end{bmatrix}, \tag{12}$$

and

$$N = \begin{bmatrix} k_{w2} w^3 \\ k_{\alpha 2}\alpha^3 \\ k_{\beta 2}\beta^3 \end{bmatrix}. \tag{13}$$

Multiplying (8) from the left by the inverse M^{-1} of M, we obtain

$$\ddot{q} = C^* \dot{q} + K^* q - M^{-1} N(q, q, q) \tag{14}$$

where $C^* = -M^{-1}C$ and $K^* = -M^{-1}K$.

In state space form, we define

$$X = \begin{bmatrix} X_1 \\ X_2 \\ X_3 \\ X_4 \\ X_5 \\ X_6 \end{bmatrix} = \begin{bmatrix} w \\ \dot{w} \\ \alpha \\ \dot{\alpha} \\ \beta \\ \dot{\beta} \end{bmatrix}. \tag{15}$$

Using these variables, (14) is rewritten as

$$\begin{bmatrix} \dot{X}_2 \\ \dot{X}_4 \\ \dot{X}_6 \end{bmatrix} = C^* \begin{bmatrix} X_2 \\ X_4 \\ X_6 \end{bmatrix} + K^* \begin{bmatrix} X_1 \\ X_3 \\ X_5 \end{bmatrix} - M^{-1} \begin{bmatrix} k_{w2} X_1^3 \\ k_{\alpha 2} X_3^3 \\ k_{\beta 2} X_5^3 \end{bmatrix}. \tag{16}$$

Additionally, we have:

$$\begin{aligned} \dot{X}_1 &= X_2, \\ \dot{X}_3 &= X_4, \\ \dot{X}_5 &= X_6. \end{aligned} \tag{17}$$

Combining these equations, we obtain the following form:

$$\dot{X} = B(U)X + N_c(X, X, X) \tag{18}$$

where $N_c(X, X, X)$ are the cubic vector functions of the state variables which describe the structural nonlinearity

$$N_c = \begin{bmatrix} 0 \\ N_{c2} \\ 0 \\ N_{c4} \\ 0 \\ N_{c6} \end{bmatrix} \tag{19}$$

and

$$B(U) = \begin{bmatrix} 0 & 1 & 0 & 0 & 0 & 0 \\ K_{11}^* & C_{11}^* & K_{12}^* & C_{12}^* & K_{13}^* & C_{13}^* \\ 0 & 0 & 0 & 1 & 0 & 0 \\ K_{21}^* & C_{21}^* & K_{22}^* & C_{22}^* & K_{23}^* & C_{23}^* \\ 0 & 0 & 0 & 0 & 0 & 1 \\ K_{31}^* & C_{31}^* & K_{32}^* & C_{32}^* & K_{33}^* & C_{33}^* \end{bmatrix}.$$

The matrix $B(U)$ has a set of six eigenvalues λ_i, $i = 1, 2, \ldots, 6$. These eigenvalues are complex conjugates ($\lambda_2 = \overline{\lambda_1}$, $\lambda_4 = \overline{\lambda_3}$, and $\lambda_6 = \overline{\lambda_5}$). The real parts of these eigenvalues correspond to the damping coefficients and the imaginary parts are the coupled frequencies of the aeroelastic system. The solution of the linear part is asymptotically stable if the real parts of the λ_i are negative. In addition, if one of the real parts is positive, the linearized system is unstable. The speed at which one or more eigenvalues have zero real parts

corresponds to the onset of the linear instability and is termed as the flutter speed, U_f.

3.2 Duhamel formulation

To simulate the arbitrary motions of the aeroelastic system, the loads associated with Theodorsen's function are replaced by the Duhamel formulation in the time domain and written as [2, 12]

$$L_c = C(k) f(t) = f(0)\phi(\tau) + \int_0^\tau \frac{\partial f(\sigma)}{\partial \sigma}\phi(\tau-\sigma)\, d\sigma \tag{20}$$

where

$$f(t) = U\alpha + \dot{w} + b\left(\frac{1}{2} - a\right)\dot{\alpha} + 1/\pi T_{10} U\beta + b\left(\frac{1}{2\pi}\right) T_{11}\dot{\beta} \tag{21}$$

and $\phi(\tau)$ is Wagner function. The Sears approximation to $\phi(\tau)$ is given by [2, 12, 14]

$$\phi(\tau) \approx c_0 - c_1 \mathrm{e}^{-c_2\tau} - c_3 \mathrm{e}^{-c_4\tau} \tag{22}$$

where $c_0 = 1$, $c_1 = 0.165$, $c_2 = 0.0455$, $c_3 = 0.335$ and $c_4 = 0.3$.

Using integration by parts and following the state space method proposed by [11, 12], (20) is rewritten as:

$$L_c = f(\tau)\phi(0) + \int_0^\tau f(\sigma)\frac{\partial \phi(\tau-\sigma)}{\partial \sigma}\, d\sigma,$$

$$L_c = (c_0 - c_1 - c_3) f(t) + c_2 c_4 (c_1 + c_3)\left(\frac{U^2}{b}\right)\bar{x} + (c_1 c_2 + c_3 c_4) U \dot{\bar{x}}. \tag{23}$$

With the introduction of two augmented variables, $x_{a1} = \bar{x}$ and $x_{a2} = \dot{\bar{x}}$, (1) is rewritten as

$$(\mathbf{M}_s - \mathbf{M}_{NC})\ddot{\mathbf{x}} + \left(\mathbf{B}_s - \mathbf{B}_{NC} - \frac{1}{2\mathbf{R}\mathbf{S}_2}\right)\dot{\mathbf{x}} + \left(\mathbf{K}_s - \mathbf{K}_{NC} - \frac{1}{2\mathbf{R}\mathbf{S}_1}\right)\mathbf{x} - \mathbf{R}\mathbf{S}_3\mathbf{x}_a = 0 \tag{24}$$

where $\mathbf{x} = [\alpha\ \beta\ w/b]^T$ and $\mathbf{x}_a = [x_{a1}\ x_{a2}]$.

The augmented state vector $\mathbf{x}_a = [\bar{x}\ \dot{\bar{x}}]$ contains the augmented variables which describe the effects of the wake dynamics of the airfoil. This vector is related to the other system parameters by the following differential equation [12]:

$$\ddot{\bar{x}} = \left[-c_2 c_4\left(\frac{U^2}{b}\right) - (c_2 + c_4)\left(\frac{U}{b}\right)\right]\mathbf{x}_a + \frac{1}{b}\mathbf{S}_1\mathbf{x} + \frac{1}{b}\mathbf{S}_2\dot{\mathbf{x}}. \tag{25}$$

Equations (24) and (25) are then rewritten in the state space form as

$$\dot{X} = A(X)X. \tag{26}$$

Details about the matrices in (24)–(26) are presented in Appendix B.

Table 1 presents a comparison of the coupled frequencies and flutter speed and frequency using the experimental parameters of Conner et al. [8] and as obtained from the above analyses. Of particular importance is the near 3-to-1 ratio of the flap frequency to the flutter frequency when using the Duhamel approach to represent the aerodynamic loads which points to the possibility of energy exchange between the flap motion and the pitch and plunge motions near flutter. As such and through this resonance, the impact of the flap motion on the wing can only be modeled by the Duhamel formulation through its wake capture component.

Table 1 Comparison of the coupled frequencies and flutter frequency and speed when using Duhamel and quasi-steady representations for the aerodynamic loads

Parameter	Duhamel	Quasi-steady
ω_{wc} (Hz)	4.38	4.38
$\omega_{\alpha c}$ (Hz)	9.15	9.15
$\omega_{\beta c}$ (Hz)	18.60	18.60
U_f (Hz)	24.8	23.56
ω_f (Hz)	6.16	5.46

4 Nonlinear analysis

For the quasi-steady approximation of the aerodynamic loads, we determine the type of bifurcation that is associated with the flutter of the aeroelastic system by computing the normal form of the bifurcation near the flutter speed U_f. Furthermore, we perform

analytical and numerical comparisons of the effects of nonlinearities when using the unsteady, based on both the Duhamel and quasi-steady, formulations. The perturbation analysis used to derive the normal form was performed using Mathematica. The Runga–Kutta method was used to perform the numerical integrations.

4.1 Normal form of Hopf bifurcation

To derive the nonlinear normal form, we first add a perturbation term, $\epsilon^2\sigma_U\ U_f$, to the flutter speed ($U = U_f + \sigma_U\epsilon^2 U_f$), which leads to the appearance of the secular terms at the third order. Taking into account the perturbation term of the flutter speed, the matrix $B(U)$ is written as the sum $B(U_f) + \epsilon^2 B_1(U_f)$, where

$$B_1(U_f) = \begin{bmatrix} 0 & 0 & 0 & 0 & 0 & 0 \\ 0 & f_2U_f & 2e_3U_f^2 & f_4U_f & 2e_5U_f^2 & f_6U_f \\ 0 & 0 & 0 & 0 & 0 & 0 \\ 0 & f_8U_f & 2e_8U_f^2 & f_{10}U_f & 2e_{10}U_f^2 & f_{12}U_f \\ 0 & 0 & 0 & 0 & 0 & 0 \\ 0 & f_{14}U_f & 2e_{13}U_f^2 & f_{16}U_f & 2e_{15}U_f^2 & f_{18}U_f \end{bmatrix}$$

and where e_i and f_i are the associated values for K^* and C^* depending, respectively, on U^2 and U as can be deduced from (10), (11) and (13).

Equation (27) is then written as

$$\dot{X} = B(U_f)X + \epsilon^2\sigma_U B_1(U_f)X + N_c(X, X, X). \quad (27)$$

Letting P be the matrix whose columns are the eigenvectors of the matrix corresponding to the eigenvalues $\pm j\omega_1 - \mu_1$, $\pm j\omega_2$, and $\pm j\omega_3 - \mu_3$ of $B(U_f)$, we define a new vector $\mathbf{Y}$ such that $X = PY$ and rewrite (27) as

$$P\dot{Y} = B(U_f)PY + \epsilon^2\sigma_U B_1(U_f)PY + N_c(PY). \quad (28)$$

Multiplying (28) from the left by the inverse P^{-1} of P, we obtain

$$\dot{Y} = JY + \epsilon^2\sigma_U GY + P^{-1}N_c(PY) \quad (29)$$

where $J = P^{-1}B(U_f)P$ is a diagonal matrix whose elements are the eigenvalues $\pm j\omega_1 - \mu_1$, $\pm j\omega_2$, and $\pm j\omega_3 - \mu_3$ of $B(U_f)$ and $G = P^{-1}B_1(U_f)P$. We note that $Y_2 = \overline{Y_1}$, $Y_4 = \overline{Y_3}$, $Y_6 = \overline{Y_5}$ and hence (29) is rewritten in component form as

$$\dot{Y}_1 = j\omega_1 Y_1 - \mu_1 Y_1 + \epsilon^2\sigma_U \sum_1^5 G_{1i}Y_i + N_1(Y, Y, Y), \quad (30)$$

$$\dot{Y}_3 = j\omega_2 Y_3 + \epsilon^2\sigma_U \sum_1^5 G_{3i}Y_i + N_3(Y, Y, Y), \quad (31)$$

$$\dot{Y}_5 = j\omega_3 Y_5 - \mu_3 Y_5 + \epsilon^2\sigma_U \sum_1^5 G_{5i}Y_i + N_5(Y, Y, Y), \quad (32)$$

where the $N_i(Y, Y, Y)$ are trilinear functions of the Y. Because we have considered only cubic nonlinearities, the solutions of Y_1 and Y_5 decay to zero. Consequently, we retain only the non-decaying solution (Y_3). Moreover, to compute the normal form of the Hopf bifurcation of (30)–(32) near $U = U_f$, we follow Nayfeh and Balachandran [15] and search for a third-order approximate solution of (31) in the following form:

$$Y_3 = \epsilon Y_{31}(T_0, T_2) + \epsilon^2 Y_{32}(T_0, T_2) + \epsilon^3 Y_{33}(T_0, T_2) + O(\epsilon^4) \quad (33)$$

where $T_n = \epsilon^n t$. In terms of the T_i, the time derivative can be expressed as

$$\frac{d}{dt} = \frac{\partial}{\partial T_0} + \epsilon^2\frac{\partial}{\partial T_2} = D_0 + \epsilon^2 D_2. \quad (34)$$

Substituting (33) and (34) into (31) and equating terms of like powers of ϵ, we obtain two different set of relations for ϵ and ϵ^3 as: Order(ϵ)

$$D_0 Y_{31} - j\omega_2 Y_{31} = 0, \quad (35)$$

Order(ϵ^3)

$$D_0 Y_{33} - j\omega_2 Y_{33} = -D_2 Y_{31} + \sigma_U G_{33} Y_{31} + N(Y_{31}, Y_{31}, \overline{Y_{31}}) + cc + NST, \quad (36)$$

where NST stands for terms that do not produce secular terms and cc stands for the complex conjugate of the preceding terms. The solution of (35) is expressed as

$$Y_{31} = A(T_2)e^{j\omega_2 T_0}. \quad (37)$$

Substituting (37) into (36) and eliminating the terms that lead to secular terms, we obtain the modulation equation

$$D_2 A = \sigma_U G_{33} A + N_e A^2 \overline{A}. \tag{38}$$

The effect of the cubic nonlinearity (k_{w2}, k_{α_2}, and k_{β_2}) on the system is expressed through N_e. For convenience, we write (38) as

$$D_2 A = \beta A + N_e A^2 \overline{A} \tag{39}$$

where $\beta = \sigma_U G_{33}$.

Expressing A in the polar form, $A(T_2) = \frac{1}{2} a e^{i\gamma(T_2)}$, and separating the real and imaginary parts in (39), we obtain the following nonlinear normal form of the Hopf bifurcation:

$$a' = \beta_r a + \frac{1}{4} N_{er} a^3, \tag{40}$$

$$\gamma' = \beta_i + \frac{1}{4} N_{ei} a^2, \tag{41}$$

where a is the amplitude and γ is the shifting angle of the periodic solution. Equation (40) has generally three equilibrium solutions which are:

$$a = 0, \; a = \pm \sqrt{\frac{-4\beta_r}{N_{er}}}.$$

The solution $a = 0$ corresponds to the fixed points $(0, 0)$. The other two solutions are the nontrivial ones. The origin is asymptotically stable for $\beta_r < 0$ or $\beta_r = 0$ and $N_{er} < 0$, unstable for $\beta_r > 0$ or $\beta_r = 0$ and $N_{er} > 0$. For the nontrivial solutions, they exist when $\beta_r N_{er} < 0$. Furthermore, they are stable (supercritical Hopf bifurcation) for $\beta_r > 0$ and $N_{er} < 0$ and unstable (subcritical Hopf bifurcation) for $\beta_r < 0$ and $N_{er} > 0$.

For the parameters of Conner et al. [8], the real parts of β and N_e are given by:

$$\begin{aligned} \beta_r &= 8.006\sigma_U, \\ N_{er} &= 3.21 \times 10^{-7} k_{w2} - 3.12 \times 10^{-4} k_{\alpha 2} \\ &\quad - 4.25 \times 10^{-5} k_{\beta 2}. \end{aligned} \tag{42}$$

We note that type of bifurcation associated with the flutter speed is dependent on the values of the nonlinear coefficients k_{w2}, k_{α_2}, and k_{β_2}.

5 Results and discussions

In this section, we compare the analytical solution as determined from the normal form of Hopf bifurcation analysis with numerical integrations of the governing equations when using the quasi-steady approximation and the Duhamel formulation. We consider three different configurations. Table 2 shows the values used for the nonlinear spring coefficients and the corresponding real part of the effective nonlinearity (N_{er}). These coefficients are chosen to yield supercritical instabilities in the first and second configurations and a subcritical instability in the third one. Furthermore, the stiffness of the plunge motion is assumed to be linear in the first configuration.

Using the nonlinear normal form, the amplitudes of the LCO for the plunge (A_w), pitch (A_α) and flap (A_β) motions are given by:

$$A_h = a\sqrt{P[1,3]_r^2 + P[1,3]_i^2}, \tag{43}$$

$$A_\alpha = a\sqrt{P[3,3]_r^2 + P[3,3]_i^2}, \tag{44}$$

$$A_\beta = a\sqrt{P[5,3]_r^2 + P[5,3]_i^2}, \tag{45}$$

where $[.]_r$ and $[.]_i$ denote the real and imaginary parts, respectively, and $P[j,k]$ denotes the component (j,k) of matrix P.

Concerning the first configuration, Fig. 2 shows the variations of the plunge, pitch and flap motions with the freestream velocity. In general the normal form yields a good prediction of the pitch and plunge motions for speeds up to $1.2U_f$. As for the flap motion, the normal form yields a good prediction of the bifurcation. However, it fails to predict the amplitudes of this motion at speeds above $1.05U_f$. We note here that we have a supercritical bifurcation (because N_{er} is negative) as predicted by the normal form.

The normal form analysis of the second configuration shows agreement between the predicted and

Table 2 Parameters of the three considered configurations

	First configuration	Second configuration	Third configuration
k_{w2}/k_{w0}	0	10	500
$k_{\alpha 2}/k_{\alpha 0}$	10	30	35
$k_{\beta 2}/k_{\beta 0}$	5	10	10
N_{er}	−0.117	−0.342	0.0429

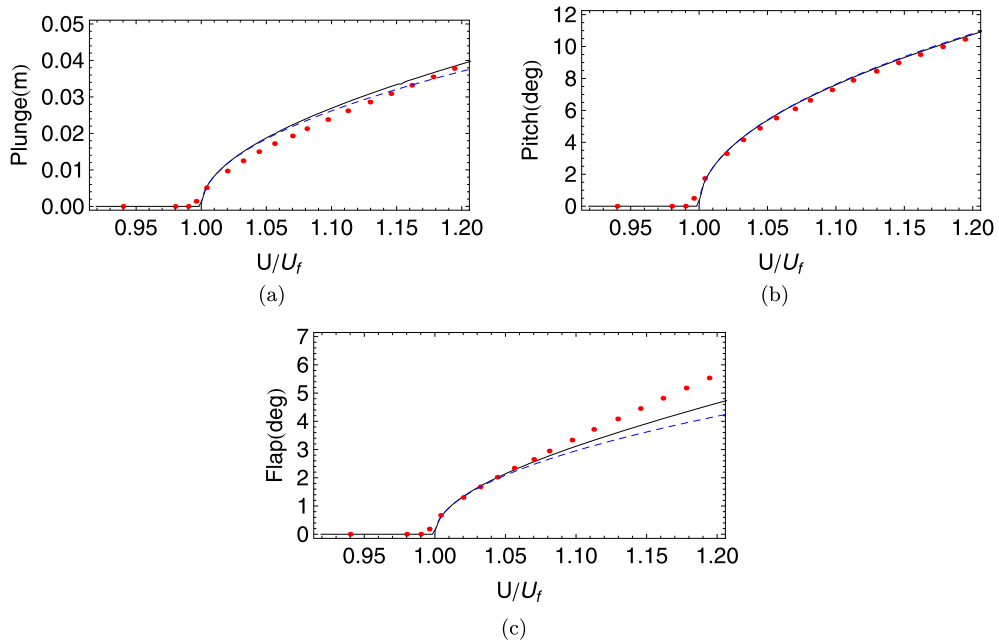

Fig. 2 Variation of the plunge (**a**), pitch (**b**), and flap (**c**) with the freestream velocity, for the first configuration, using the normal form based on the quasi steady formulation (*dashed lines*) and numerical integrations of the quasi-steady approximation (*solid lines*) and Duhamel formulation (*dots*)

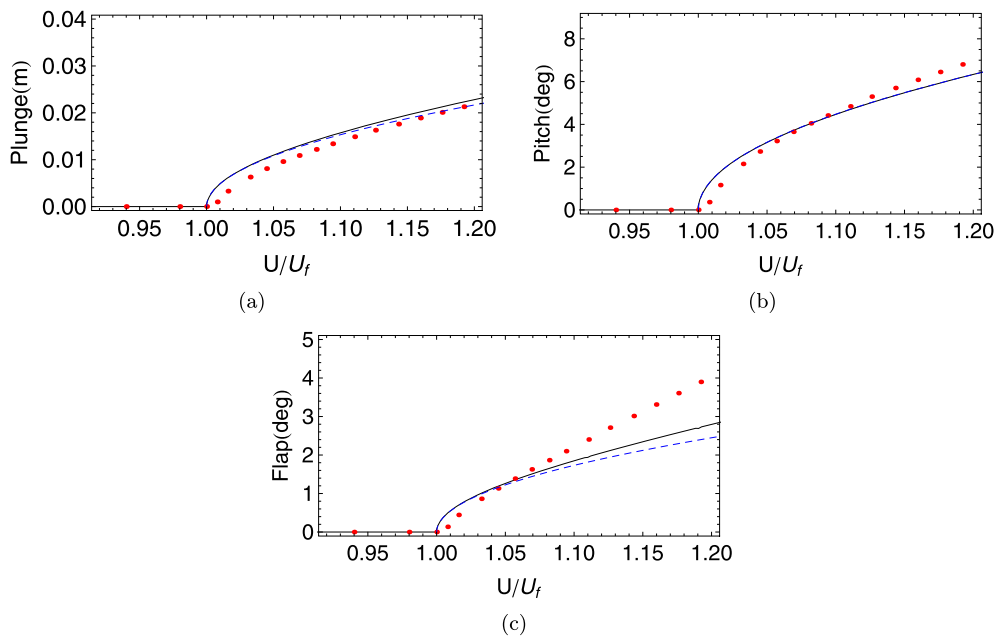

Fig. 3 Variation of the plunge (**a**), pitch (**b**), and flap (**c**) with the freestream velocity, for the second configuration, using the normal form based on the quasi-steady formulation (*dashed lines*) and numerical integrations of the quasi-steady approximation (*solid lines*) and Duhamel formulation (*dots*)

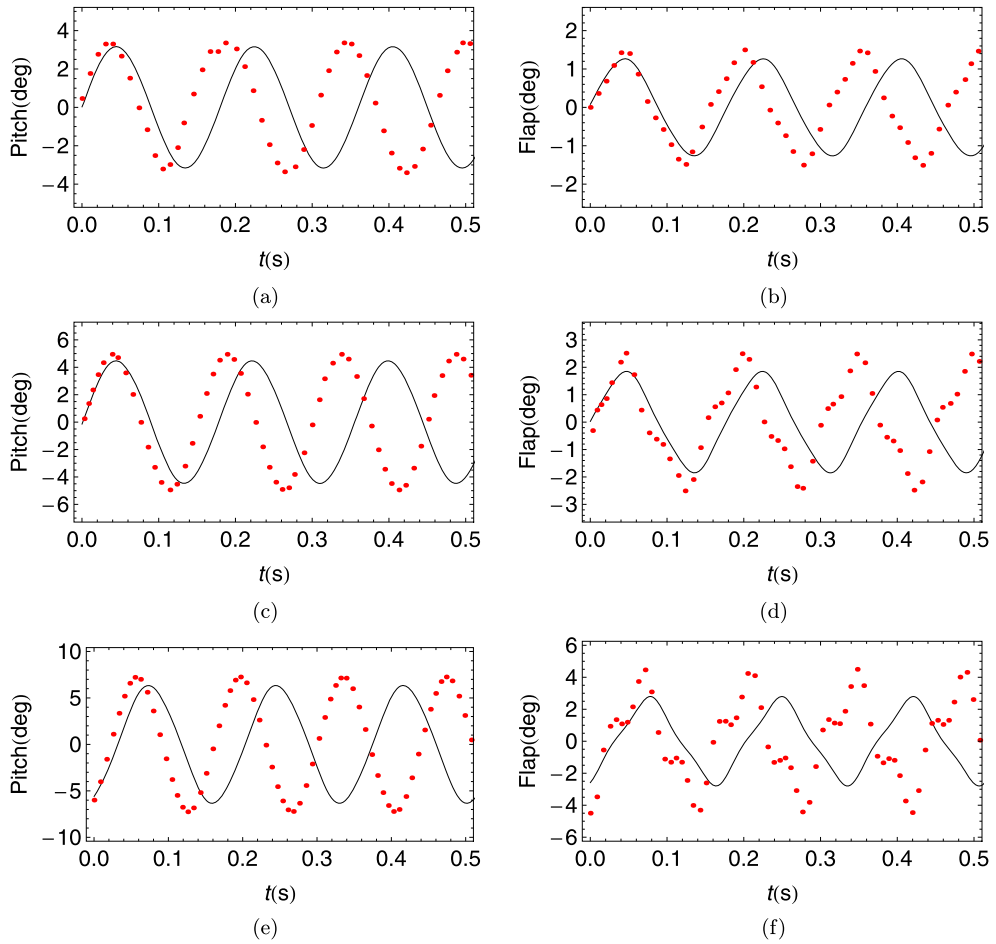

Fig. 4 Time histories of the pitch (**a**, **c** and **e**) and flap (**b**, **d** and **f**), for the second configuration, for the different used methods (*dots* for the numerical integrations of the Duhamel representation and *solid line* for the numerical integrations of the quasi-steady approximation) when $U = 1.05U_f$ (**a** and **b**), $U = 1.1U_f$ (**c** and **d**) and $U = 1.2U_f$ (**e** and **f**)

numerically determined amplitudes of the pitch and plunge motions. On the other hand, the normal form analysis fails to predict the amplitude of the flap motion at speeds above $1.05U_f$, as shown in Fig. 3. Time histories of the predicted motions using the Duhamel and quasi-steady formulations at different freestream velocities are shown in Fig. 4. The results show that predicted pitch motions by both analyses are periodic, as shown in Figs. 4(a), (c) and (e), while the amplitudes of the predicted motions are about the same, their frequencies are different. This is expected from the linear analysis presented in Table 1. As for the predicted flap motions, the results show significant differences when using the two approaches. At the relatively lower speeds, $U = 1.05U_f$, near the bifurcation the flap motion contains mostly one frequency component, as shown in Fig. 4(b). In contrast, this motion contains other frequencies components at the higher speeds, as shown in Figs. 4(d) and (f). This is clearly due to the ability of the Duhamel formulation to capture the dynamic wake effects of the flap.

Power spectra of the pitch and flap motions when using the Duhamel formulation for the aerodynamic loads are shown in Fig. 5. We note the two peaks near the flutter and flap frequencies which have a 3-to = 1 ratio for the three considered freestream velocities. For the pitch motion, we note that dominant peak is that of the flutter frequency of the wing as shown in Figs. 5(a), (c) and (e). Regarding the flap motions, it is noted that the amplitude of the flap frequency increases signifi-

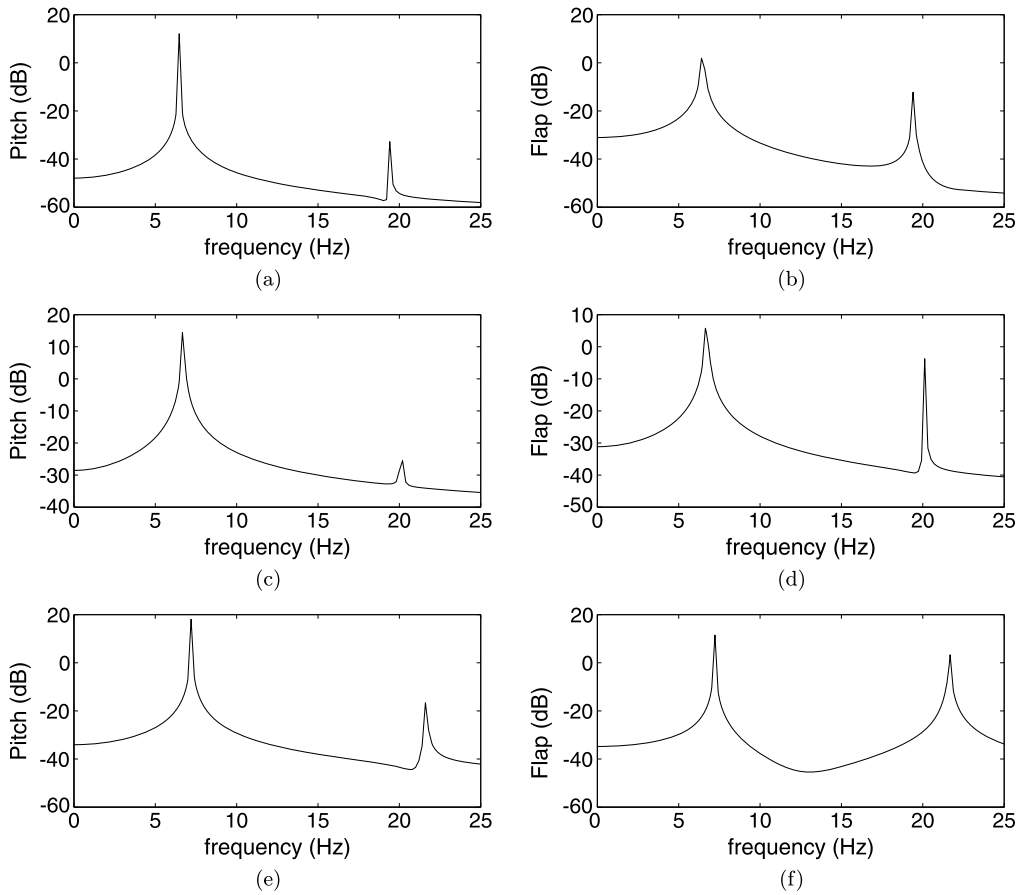

Fig. 5 Power spectrum for the pitch (**a**, **c** and **e**) and flap (**b**, **d** and **f**), for the second configuration, for the Duhamel representation when $U = 1.05U_f$ (**a** and **b**), $U = 1.1U_f$ (**c** and **d**) and $U = 1.2U_f$ (**e** and **f**)

cantly as the freestream velocity is increased, as shown in Figs. 5(b), (d) and (f). Again, this behavior is due to the 3-to-1 ratio of the coupled flap and flutter frequencies, as shown in Table 1. As expected, there is more energy transfer to the flap motion when increasing the freestream velocity.

Figure 6 shows the time histories for the pitch and flap motions for the quasi-steady approximation for the third configuration. We note that both motions are periodic. On the other hand, when using the Duhamel representation, we obtain nonperiodic/chaotic motions as shown in Fig. 7 for both pitch and flap responses. This is determined from the Poincaré sections shown in Fig. 8. Therefore, for the considered subcritical configuration, the quasi-steady approximation failed to predict the arbitrary and nonperiodic motions that are associated with the dynamic effects of the flap.

Variations of the root mean square (RMS) values of the plunge, pitch and flap with forward and backward sweeps of the freestream velocity for the third (subcritical) configuration presented in Table 2 as predicted by the quasi-steady approximation are shown in Fig. 9. Clearly, a hysteretic response is identified. This hysteresis is a characteristic of the subcritical instability. As such, this result is in agreement with values obtained from normal form analysis of Hopf bifurcation. The plotted curves in Fig. 10 show the bifurcation diagram for the third configuration when using the Duhamel representation approach for the aerodynamic loads. Again, we note that the hysteresis in the response is caused by the subcritical instability of the system. However, we note that there is a large difference in the maximum values for all system outputs when considering the quasi-steady approximation and the Duhamel formulation. For the Duhamel formula-

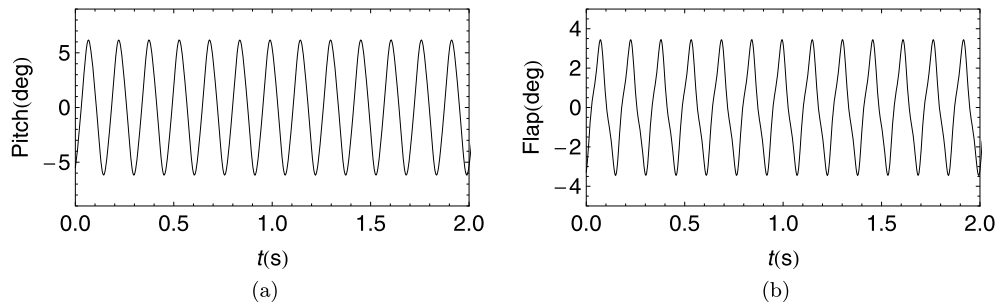

Fig. 6 Time histories of the pitch (**a**) and flap (**b**), for the third configuration, for the quasi-steady representation when $U = 1.05U_f$

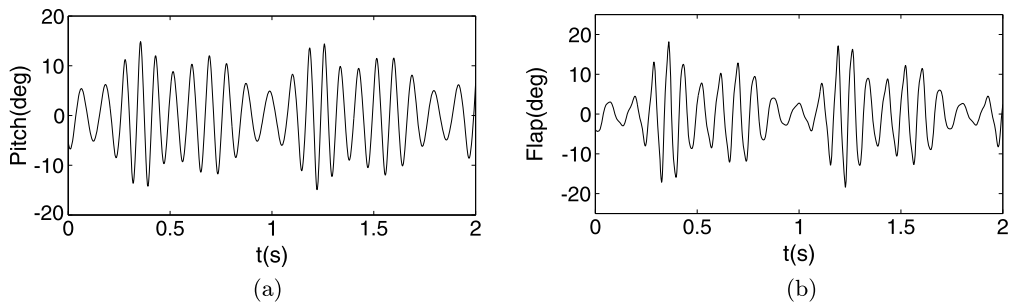

Fig. 7 Time histories of the pitch (**a**) and flap (**b**), for the third configuration, for the Duhamel representation when $U = 1.05U_f$

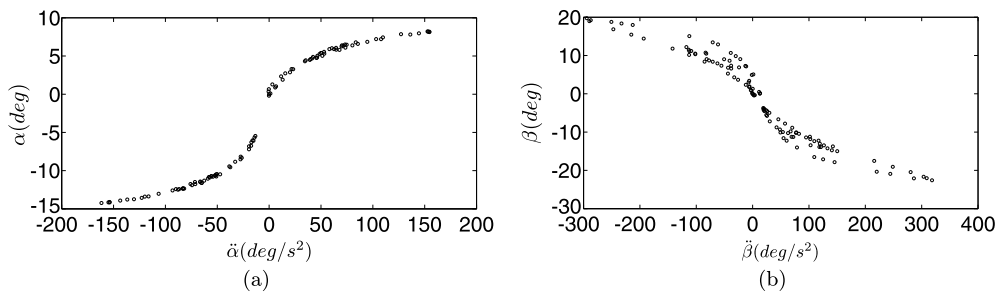

Fig. 8 Poincaré sections for the pitch (**a**) and flap (**b**), for the third configuration, for the Duhamel representation when $U = 1.05U_f$

tion of aerodynamic loads, higher pitch and flap amplitudes are obtained.

6 Conclusions

In this work, a nonlinear analysis of a three-degree-of-freedom airfoil section is performed. To study the effects of concentrated structural nonlinearities, we considered three configurations for concentrated nonlinearities in the stiffness of the pitch, plunge, and flap springs. We used two different approaches to represent the aerodynamic loads, namely, the quasi-steady approximation and the Duhamel formulation. For the wing and flap considered parameters, the linear analysis shows a difference in the predicted flutter frequencies when using the two approaches. Particularly, the Duhamel formulation shows a possibility for energy exchange between the wing and flap through a 3-to-1 resonance mechanism. Using the quasi-steady approximation, we derived the normal form of Hopf bifurcation to characterize the system's stability and the response near the bifurcation. The results show that both the quasi-steady approximation and the unsteady representation, which is based on the Duhamel formulation, yield comparable results when the pitch

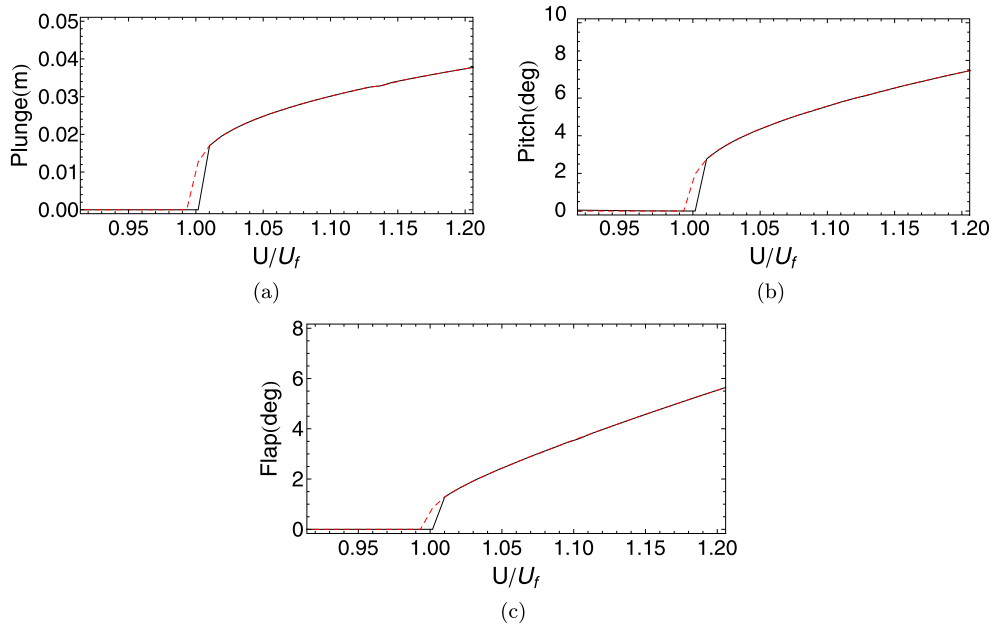

Fig. 9 Variation of the RMS values for the plunge (**a**), pitch (**b**), and flap (**c**) with the freestream velocity, for the third configuration, for the quasi-steady approximation (*dashed lines* for the decreasing speeds and *solid line* for the increasing speeds)

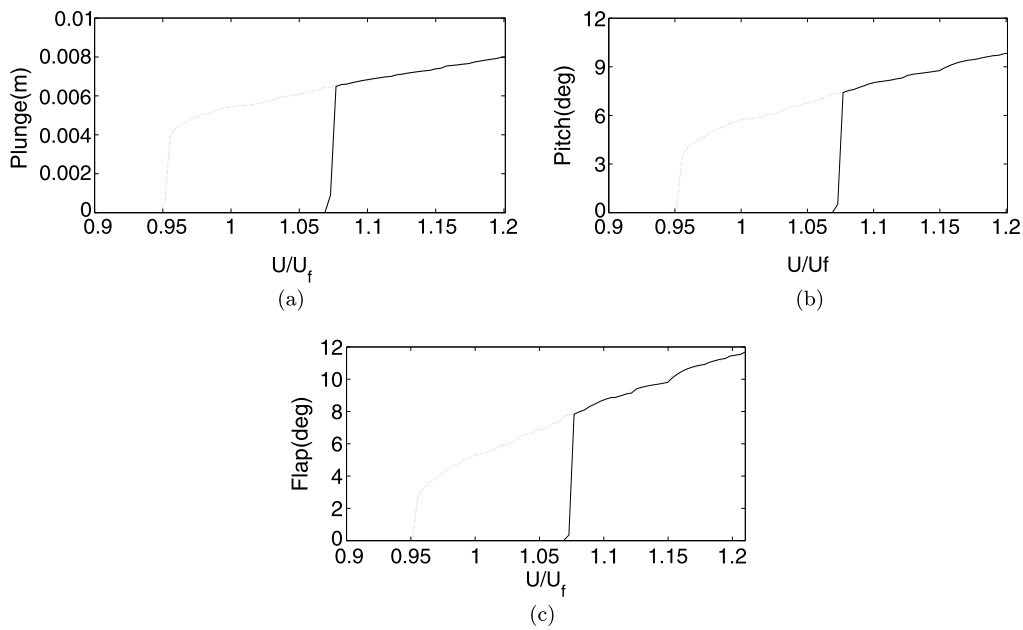

Fig. 10 Variation of the RMS values for the plunge (**a**), pitch (**b**), and flap (**c**) with the freestream velocity, for the third configuration, for the Duhamel approximation (*dashed lines* for the decreasing speeds and *solid line* for the increasing speeds)

and plunge motions are periodic. However, the two approaches yield different amplitudes for the flap motions at higher speeds (above $1.05U_f$). This is due to the failure of the quasi-steady approach to account for the dynamic wake effects of the flap. For the same reason, the quasi-steady approach fails to predict non-periodic or chaotic motions that are associated with subcritical instabilities. These results show the impor-

tance of correctly modeling the aerodynamic loads when characterizing complex phenomena associated with nonlinearities in aeroelastic systems.

Acknowledgement The authors acknowledge the financial support of the Sao Paulo State Research Agency, FAPESP, Brazil (Grant 2007/08459-1) and the Coordination for the Improvement of Higher Education Personnel (CAPES), Brazil (Grant 0205109).

Appendix A: Theodorsen constants

$$T_1 = -\frac{2+c^2}{3}\sqrt{1-c^2} + c\cos^{-1}c,$$

$$T_3 = -\frac{1-c^2}{8}\left(5c^2+4\right) + \frac{1}{4}c\left(7+2c^2\right), \times\sqrt{1-c^2}\cos^{-1}c - \left(\frac{1}{8}+c^2\right)\left(\cos^{-1}c\right)^2,$$

$$T_4 = c\sqrt{1-c^2} - \cos^{-1}c,$$

$$T_5 = -\left(1-c^2\right) - \left(\cos^{-1}c\right)^2 + 2c\sqrt{1-c^2}\cos^{-1}c,$$

$$T_7 = c\frac{7+2c^2}{8}\sqrt{1-c^2} - \left(\frac{1}{8}+c^2\right)\cos^{-1}c,$$

$$T_8 = -\frac{1}{3}\left(1+2c^2\right)\sqrt{1-c^2} + c\cos^{-1}c,$$

$$T_9 = \frac{1}{2}\left[\frac{\sqrt{1-c^2}(1-c^2)}{3} + aT_4\right],$$

$$T_{10} = \sqrt{1-c^2} + \cos^{-1}c,$$

$$T_{11} = (2-c)\sqrt{1-c^2} - (1-2c)\cos^{-1}c,$$

$$T_{12} = (2+c)\sqrt{1-c^2} - (1+2c)\cos^{-1}c,$$

$$T_{13} = -\frac{1}{2}[T_7 + (c-a)T_1].$$

Appendix B: Matrices of (24) and (26)

$$\mathbf{M}_s = \begin{bmatrix} r_\alpha^2 & r_\beta^2 + (c-a)x_\beta & x_\alpha \\ r_\beta^2 + (c-a)x_\beta & r_\beta^2 & x_\beta \\ x_\alpha & x_\beta & M_T/m_W \end{bmatrix},$$

$$\mathbf{B}_s = (\mathbf{\Lambda}^T)^{-1}\begin{bmatrix} 2m_\alpha\omega_\alpha\xi_\alpha & 0 & 0 \\ 0 & 2m_\beta\omega_\beta\xi_\beta & 0 \\ 0 & 0 & 2m_w\omega_w\xi_w \end{bmatrix}\mathbf{\Lambda}^{-1},$$

where m_α, m_β, m_w are modal masses.

$$\mathbf{K}_s = \begin{bmatrix} r_\alpha^2\omega_\alpha^2 & 0 & 0 \\ 0 & r_\beta^2\omega_\beta^2 F(\beta)/\beta & 0 \\ 0 & 0 & \omega_w^2 \end{bmatrix},$$

$$\mathbf{M}_{NC} = -\frac{\rho}{m_W}\begin{bmatrix} \pi b^2(\frac{1}{8}+a^2) & -(T_7+(c-a)T_1)b^2 & -\pi ab^2 \\ 2T_{13}b^2 & -T_3b^2/\pi & -T_1b^2 \\ -\pi ab^2 & -T_1b^2 & \pi b^2 \end{bmatrix},$$

$$\mathbf{B}_{NC} = -\frac{\rho}{m_W}\begin{bmatrix} \pi(\frac{1}{2}-a)Ub & T_1 - T_8 - (c-a)T_4 + T_{11}/2)Ub & 0 \\ (-2T_9 - T_1 + T_4(a-\frac{1}{2}))Ub & -T_4T_{11}Ub/(2\pi) & 0 \\ \pi Ub & -UT_4b & 0 \end{bmatrix},$$

$$\mathbf{K}_{NC} = -\frac{\rho}{m_W}\begin{bmatrix} 0 & (T_4+T_{10})U^2 & 0 \\ 0 & (T_5 - T_4T_{10})U^2/\pi & 0 \\ 0 & 0 & 0 \end{bmatrix},$$

$$\mathbf{R} = \begin{bmatrix} 2\pi\rho U(a+\frac{1}{2})/m_W & -\rho UT_{12}/m_W & -\frac{2\pi\rho U}{m_W} \end{bmatrix}^T,$$

$$\mathbf{S}_1 = \begin{bmatrix} U & T_{10}U/\pi & 0 \end{bmatrix},$$

$$\mathbf{S}_2 = \begin{bmatrix} b\left(\frac{1}{2} - a\right) & bT_{11}/2\pi & b \end{bmatrix},$$

$$\mathbf{S}_3 = \begin{bmatrix} c_2c_4(c_1 + c_3)U^2/b & (c_1c_2 + c_3c_4)U \end{bmatrix},$$

$$\mathbf{A} = \begin{bmatrix} \mathbf{0} & \mathbf{I}_{3x3} & \mathbf{0} \\ -\mathbf{M}_t^{-1}\mathbf{K}_t & -\mathbf{M}_t^{-1}\mathbf{B}_t & -\mathbf{M}_t^{-1}\mathbf{D} \\ \mathbf{E}_1 & \mathbf{E}_2 & \mathbf{F} \end{bmatrix}$$

being,

$$\mathbf{M}_t = \mathbf{M}_s - \mathbf{M}_{NC}, \qquad \mathbf{B}_t = \mathbf{B}_s - \mathbf{B}_{NC} - 1/2\mathbf{RS}_2, \qquad \mathbf{K}_t = \mathbf{K}_s - \mathbf{K}_{NC} - 1/2\mathbf{RS}_1, \qquad \mathbf{D} = \mathbf{RS}_3,$$

$$\mathbf{E}_1 = \begin{bmatrix} 0 & 0 & 0 \\ U/b & UT_{10}/(\pi b) & 0 \end{bmatrix},$$

$$\mathbf{E}_2 = \begin{bmatrix} 0 & 0 & 0 \\ (1/2 - a) & T_{11}/(2\pi) & 1 \end{bmatrix},$$

$$\mathbf{F} = \begin{bmatrix} 0 & 1 \\ -c_2c_4U^2/b & -(c_2 + c_4)U/b \end{bmatrix}.$$

References

1. Fung, Y.C.: An Introduction to the Theory of Aeroelasticity. Dover, New York (1993)
2. Li, D., Guo, S., Xiang, J.: Aeroelastic dynamic response and control of an airfoil section with control surface nonlineatities. J. Sound Vib. **329**, 4756–4771 (2010)
3. Hodges, D.H., Pierce, G.A.: Introduction to Structural Dynamics and Aeroelasticity. Cambridge University Press, Cambridge (2002)
4. Woolston, D.S., Runyan, H., Byrsdsong, T.: Some effects of system nonlinearities in the problem of aircraft flutter. NACA Technical Report, 3539 (1955)
5. Woolston, D.S.: An investigation of effects of certain types of structural nonlinearities on wing and control surface flutter. J. Aeronaut. Sci. **24**, 1936–9956 (1957)
6. Shen, S.F., Hsu, C.C.: Analytical results of certain nonlinear flutter problems. J. Aeronaut. Sci. **25**, 136–137 (1958)
7. O'Neil, T.: Nonlinear aeroelastic response-analyses and experiments. In: Proceedings of the 34th AIAA, Aerospace Sciences Meeting and Exhibit, Reno, NV (1996)
8. Conner, M.D., Tang, D.M., Dowell, E.H., Virgin, L.N.: Nonlinear behavior of a typical airfoil section with control surface freeplay. J. Fluids Struct. **11**, 89–109 (1996)
9. Trickey, T., Virgin, L.N., Dowell, H.: The stability of limit-cycle oscillations in a nonlinear aeroelastic system. Proc. R. Soc., Math. Phys. Eng. Sci. **458**, 2203–2226 (2002)
10. Lee, B.H.K., Lui, L., Chung, K.W.: Airfoil motion in subsonic flow with strong cubic nonlinear restoring forces. J. Sound Vib. **281**, 699–717 (2005)
11. Abdelkefi, A., Nayfeh, A.H., Hajj, M.R.: Modeling and analysis of piezoaeroelastic energy harvesters. Nonlinear Dyn. (2011). doi:10.1007/s11071-011-0035-1
12. Trickey, T.: Global and local dynamics of an aeroelastic system with a control surface freeplay nonlinearity. Ph.D. Thesis, Duke University (2000)
13. Theodorsen, T.: General theory of aerodynamic instability and the mechanism of flutter. NACA Technical Report 496 (1935)
14. Lee, B.H.K., Gong, L., Wong, Y.S.: Analysis and computation of nonlinear dynamic response of a two degree of freedom system and its application in aeroelasticity. J. Fluids Struct. **11**, 225–246 (1997)
15. Nayfeh, A.H., Balachandran, B.: Applied Nonlinear Dynamics. Wiley, New York (1995)